11362 *Inorg. Chem.* **2010**, *49*, 11362–11369
DOI: 10.1021/ic101208q

Inorganic Chemistry
Article

Relationship between Cation Arrangement and Photocatalytic Activity for Sr−Al−Nb−O Double Perovskite

Hironori Iwakura,[†] Hisahiro Einaga,[‡] and Yasutake Teraoka*[,‡]

[†]*Department of Molecular and Material Sciences, Interdisciplinary Graduate School of Engineering Sciences, Kyushu University, Kasuga, Fukuoka 816-8580, Japan, and* [‡]*Department of Energy and Material Sciences, Faculty of Engineering Sciences, Kyushu University, Kasuga, Fukuoka 816-8580, Japan*

Received June 17, 2010

The relationship between the photocatalytic activity and the arrangement of metal cations was investigated with Sr−Al−Nb−O double perovskite (SAN) synthesized at 1400 °C for various calcination times using a solid state reaction. Transmission electron microscopic observation revealed that SAN particles had a domain structure of completely B-site ordered (Sr_2AlNbO_6) and disordered ($SrAl_{0.5}Nb_{0.5}O_3$) phases. The ordered phase fraction was determined using a newly proposed mixed-phase model for the Rietveld refinement and a method using the relative intensity of the superlattice line of powder X-ray diffraction. It turned out that the mass fraction of the ordered phase in SAN calcined at 1400 °C could be controlled by the calcination time as 33% (10 h), 37% (20 h), 44% (30 h), and 48% (50 h). Photocatalytic activities of SAN for the evolution of H_2 and O_2 respectively from aqueous solutions of methanol and AgF decreased with increasing the calcination time, that is, with increasing the fraction of the ordered phase. These results suggested that the photocatalytic activity of ordered Sr_2AlNbO_6 should be lower than that of disordered $SrAl_{0.5}Nb_{0.5}O_3$. This is practically the first report to reveal the photocatalytic activity of SAN as well as the effect of cation ordering in oxides on the photocatalytic activity.

1. Introduction

Photocatalysis over semiconductors has been widely studied in order to apply the reaction to efficient utilization of solar energy for water splitting, and many kinds of semiconductors have been developed.[1,2] The mechanism of heterogeneous photocatalysis by a semiconductor is described below.[3] Electron−hole pairs are initially generated in the semiconductor particles using light absorption with an energy equal to or greater than the band gap of the semiconductor. After the separation of the photogenerated electrons and holes, they migrate to the surface of the semiconductor, and the redox reactions between photogenerated carriers and adsorbed reactants proceed. According to the reaction mechanism, the photogeneration of electrons and holes and their migration in a semiconductor is the most significant process in governing its photocatalytic properties. Therefore, the bulk structure is one of the important factors for a semiconductor photocatalyst. So far, much research has been performed to investigate the relationship between the bulk structure and photocatalytic activity of semiconductors, and in many cases, the photocatalytic activity has depended on the bulk structure of the catalytic materials. For example, the photocatalytic activity has decreased with increasing the amount of lattice defects in TiO_2[4] and $BaTi_4O_9$.[5] In other research, the effects of the crystal systems and of the crystal forms on the photocatalytic activity have been investigated for A^+TaO_3 ($A^+ = Li^+, Na^+, K^+$),[6] $A^{2+}In_{0.5}Nb_{0.5}O_3$ ($A^{2+} = Ba^{2+}, Sr^{2+}, Ca^{2+}$),[7] TiO_2,[8] $BaTa_2O_6$,[9] and $La_3B^{5+}O_7$ ($B^{5+} = Nb^{5+}, Ta^{5+}$).[10] On the other hand, the effect of the cation arrangement in a semiconductor on its photocatalytic activity has been rarely investigated. The effect of cation arrangement on the photocatalytic activity of $La_3B^{5+}O_7$ ($B^{5+} = Nb^{5+}, Ta^{5+}$) was suggested,[10] but both the cation arrangement and the crystal form changed in these materials. Therefore, the effect of cation arrangement on photocatalytic activity has not been clarified in a strict sense.

*To whom correspondence should be addressed. Tel.: +81-92-583-7526. Fax: +81-92-583-8853. E-mail: teraoka.yasutake.329@m.kyushu-u.ac.jp.

(1) Osterloh, E. F. *Chem. Mater.* **2008**, *20*, 35–54.
(2) Kudo, A.; Miseki, Y. *Chem. Soc. Rev.* **2009**, *38*, 253–278.
(3) Linsebigler, L. A.; Lu, G., Jr.; Yates, T. *J. Chem. Rev.* **1995**, *95*, 735–758.
(4) Ikeda, S.; Sugiyama, N.; Murakami, S.; Kominami, H.; Kera, Y.; Noguchi, H.; Uosaki, K.; Torimoto, T.; Ohtani, B. *Phys. Chem. Chem. Phys.* **2003**, *5*, 778–783.
(5) Yamashita, Y.; Yoshida, K.; Kakihana, M.; Uchida, S.; Sato, T. *Chem. Mater.* **1999**, *11*, 61–66.
(6) Kato, H.; Kudo, A. *J. Phys. Chem. B* **2001**, *105*, 4285–4292.
(7) Yin, J.; Zou, Z.; Ye, J. *J. Phys. Chem. B* **2003**, *107*, 61–65.
(8) Torimoto, T.; Nakamura, N.; Ikeda, S.; Ohtani, B. *Phys. Chem. Chem. Phys.* **2002**, *4*, 5910–5914.
(9) Kato, H.; Kudo, A. *Chem. Phys. Lett.* **1998**, *295*, 487–492.
(10) Abe, R.; Higashi, M.; Sayama, K.; Abe, Y.; Sugihara, H. *J. Phys. Chem. B* **2006**, *110*, 2219–2226.

Published on Web 11/15/2010

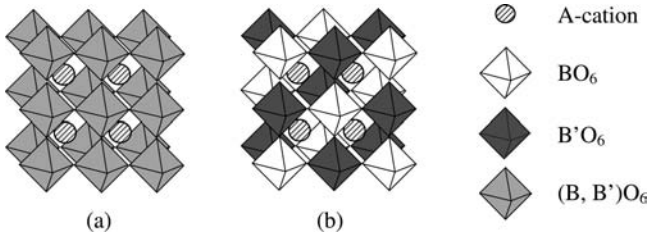

Figure 1. Cation arrangements at the B site in double perovskite. (a) Random arrangement, (b) rock-salt ordered arrangement.

Perovskite-type oxides have a general formula of ABO_3. In this structure, A and B cations are 12-fold and 6-fold coordinated with oxygen anions, respectively. Important aspects of perovskite-type oxide include the facts that most of the metal cations are known to be stably incorporated into the structure and the metal cations that occupy the A and B site can be partially substituted by other metal cations. The variety in material design for perovskite-type oxides results in a variety of functional properties.[11] Double perovskite, in which two kinds of metal cations occupy the B site at the same molar ratio, is well-known as a subclass of perovskite-type oxide. It is known that two kinds of arrangements of B cations are possible in double perovskite, random ($AB_{0.5}B'_{0.5}O_3$) and rock-salt ordering ($A_2BB'O_6$), as shown in Figure 1.[12] The differences in charge and size of the B cations are important factors for the prediction of the arrangement, and the large differences in charge and size favor the ordered arrangement of B cations. When the difference in charge of B cations is equal to or larger than three, the formation of the ordered phase has priority. In the case where the difference is two, a partially ordered arrangement of B cations has occurred,[13−18] and the degrees of cation-ordering have been changed by calcination conditions without changing the crystal structure in some kinds of oxides.[17,18] So far, several kinds of perovskite-type oxides including double perovskites have been reported as photocatalysts.[6,7,19−22] However, the relationship between cation arrangement and photocatalytic activity has not been investigated.

Photocatalytic activities of mixed metal oxides containing Nb^{5+}, Ta^{5+}, or Ti^{4+} cations have been widely investigated, and many of the oxides have been revealed to be active photocatalysts. In addition to the oxides listed above,[5−10] photocatalytic properties of the following oxides were reported: $A^+_4Nb_6O_{17}$ ($A^+ = K^+$, Rb^+),[23,24] $Bi_2M^{3+}NbO_7$ ($M^{3+} = Al^{3+}$, Ga^{3+}, In^{3+}),[25] $NaB^{5+}O_3$ ($B^{5+} = Nb^{5+}$, Ta^{5+}),[26,27] $K_2Ta_2O_6$,[27] $A_mB_mO_{3m+2}$ (m = 4, 5; A = Ca^{2+}, Sr^{2+}, La^{3+}; B = Nb^{5+}, Ti^{4+}),[28] $Sr_mTa_nO_{(m+5n/2)}$ (m = 1, 4, 5; n = 2, 4),[29] $SrTiO_3$,[30] and $BaTi_4O_9$.[31] Therefore, a double perovskite containing one of these cations must be a good candidate material for the present purpose of investigating the effect of cation arrangement on photocatalytic activity.

In this paper, Sr−Al−Nb−O double perovskites (SAN), in which Al^{3+} and Nb^{5+} cations occupy B sites, with various degrees of cation-ordering have been synthesized, and their photocatalytic properties have been investigated in relation with cation arrangement.

2. Experimental Section

2.1. Catalyst Preparation. Polycrystalline powder of Sr−Al−Nb−O double perovskite (SAN) was synthesized using a conventional solid-state reaction method. $SrCO_3$ (purity: > 99.9%, Kanto Chem. Co., Inc.), Al_2O_3 (>99.9%, Aldrich Chem. Co.), and Nb_2O_5 (>99.9%, Kishida Chem. Co., Ltd.) were used as starting materials. $SrCO_3$ (2.955 g), Al_2O_3 (0.510 g), Nb_2O_5 (1.330 g), and ethanol (5 mL) were added into a zirconia pot (45 mL), and the mixture was then ground by a planetary ball mill at 500 rpm for 5 h (Fritsch, pulverizette-7). After drying the mixture, the powder was calcined in the air under appropriate conditions with intermediate grindings every 10 h. TiO_2 powder (P25) was supplied from the Catalysis Society of Japan as a reference catalyst, JRC-TIO-4.

RuO_2 was supported on SAN by using an impregnation method according to a procedure reported earlier.[32] SAN (1.0 g) was suspended in tetrahydrofuran (THF, 100 mL) using magnetic stirring. Separately, $Ru_3(CO)_{12}$ (purity >95%, Wako Pure Chem. Industries, Ltd.) was dissolved in THF with a concentration of 2.8×10^{-5} mol Ru mL^{-1}, and the solution (2.7 mL) was added into the suspension. After evaporation to dryness at 80 °C, the obtained powder was calcined at 400 °C for 5 h in the air to form RuO_2 supported on SAN.

2.2. Characterization of Catalyst. The crystal structure of the catalyst was examined using powder X-ray diffraction (PXRD) measurement using Cu Kα radiation (Rigaku RINT-2200, 40 kV, 20 mA) and transmission electron microscopy (TEM; JEOL JEM-2000EX/T, accelerating voltage: E = 200 kV). Rietveld analysis using a PXRD pattern was performed to refine the crystal structure. The RIETAN-2000 program[33] was used for the structural refinement, and a pseudo-Voigt peak-shape function was used as a profile function. For the refinement of a crystal structure, the PXRD pattern was measured at room temperature using the fixed time mode over an angular range of $10 \leq 2\theta/^\circ \leq 140$ with a 0.02° (2θ) step and a counting time of 1.5−3.0 s. Space groups reported in a previous paper[12] were used for the refinement.

The UV−vis diffuse reflectance spectrum (UV−vis DRS) of the sample was measured using a Shimadzu UV-3100 equipped

(11) Pea, A. M.; Fierro, G. L. *J. Chem. Rev.* **2001**, *101*, 1981–2017.
(12) Anderson, T. M.; Greenwood, B. K.; Taylor, A. G.; Poeppelmeier, R. K. *Prog. Solid State Chem.* **1993**, *22*, 197–233.
(13) Choy, J. H.; Hong, S. T.; Choi, K. S. *J. Chem. Soc., Faraday Trans.* **1996**, *92*, 1051–1059.
(14) Kawano, T.; Takahashi, J.; Yamada, T.; Yamane, H. *J. Ceram. Soc. Jpn.* **2007**, *115*, 792–796.
(15) Faik, A.; Gateshki, M.; Igartua, M. J.; Pizarro, L. J.; Insausti, M.; Kaindl, R.; Grzechnik, A. *J. Solid State Chem.* **2008**, *181*, 1759–1766.
(16) Mandal, K. T.; Poltavets, V. V.; Croft, M.; Greenblatt, M. *J. Solid State Chem.* **2008**, *181*, 2325–2331.
(17) Woodward, P.; Hoffmann, R.-D.; Sleight, W. A. *J. Mater. Res.* **1994**, *9*, 2118–2127.
(18) Setter, N.; Cross, E. L. *J. Mater. Sci.* **1980**, *15*, 2478–2482.
(19) Wrighton, S. M.; Ellis, B. A.; Wolczanski, T. P.; Morse, L. D.; Abrahamson, B. H.; Ginley, S. D. *J. Am. Chem. Soc.* **1976**, *98*, 2774–2779.
(20) Kato, H.; Kobayashi, H.; Kudo, A. *J. Phys. Chem. B* **2002**, *106*, 12441–12447.
(21) Li, D.; Zheng, J.; Zou, Z. *J. Phys. Chem. Solids* **2006**, *67*, 801–806.
(22) Hatakeyama, T.; Takeda, S.; Ishikawa, F.; Ohmura, A.; Nakayama, A.; Yamada, Y.; Mathusima, A.; Yea, J. *J. Ceram. Soc. Jpn.* **2010**, *118*, 91–95.
(23) Kudo, A.; Tanaka, A.; Domen, K.; Maruya, K.; Aika, K.; Onishi, T. *J. Catal.* **1988**, *111*, 67–76.
(24) Sayama, K.; Arakawa, H.; Domen, K. *Catal. Today* **1996**, *28*, 175–182.
(25) Zou, Z.; Ye, J.; Arakawa, H. *Chem. Phys. Lett.* **2001**, *333*, 57–62.
(26) Saito, K.; Kudo, A. *Inorg. Chem.* **2010**, *49*, 2017–2019.
(27) Ishihara, T.; Baik, S. N.; Ono, N.; Nishiguchi, H.; Takita, Y. *J. Photochem. Photobiol. A* **2004**, *167*, 149–157.
(28) Kim, G. H.; Hwang, W. D.; Kim, J.; Kim, G. Y.; Lee, S. J. *Chem. Commun.* **1999**, 1077–1078.
(29) Yoshioka, K.; Petrykin, V.; Kakihana, M.; Kato, H.; Kudo, A. *J. Catal.* **2005**, *232*, 102–107.
(30) Domen, K.; Kudo, A.; Onishi, T. *J. Catal.* **1986**, *102*, 92–98.
(31) Inoue, Y.; Asai, Y.; Sato, K. *J. Chem. Soc., Faraday Trans.* **1994**, *90*, 797.
(32) Ogura, S.; Sato, K.; Inoue, Y. *Phys. Chem. Chem. Phys.* **2000**, *2*, 2449–2454.
(33) Izumi, F.; Ikeda, T. *Mater. Sci. Forum* **2000**, *198*, 321–324.

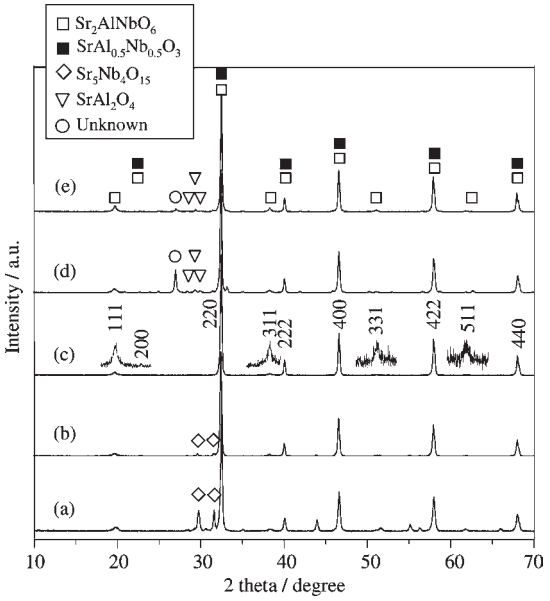

Figure 2. PXRD patterns of Sr−Al−Nb−O double perovskites calcined at various temperatures. Starting solid-state mixture was directly calcined for 10 h at (a) 1200 °C, (b) 1300 °C, (c) 1400 °C, and (d) 1500 °C. (e) After calcination of sample c at 1500 °C for 10 h.

with an integrating sphere attachment. α-Al_2O_3 powder was used as a reference sample. The mixture of SAN and Al_2O_3 (10 wt % SAN/Al_2O_3) powders was used to obtain a reflectance spectrum. A reflectance spectrum was collected over wavelengths from 800 to 220 nm with a 0.5 nm step. The reflectance was transformed into the Kubelka−Munk function. Photon energy at the absorption edge was estimated by extrapolating the linearly ascending portion of the spectrum to the *x* axis, and the value was defined as an optical band gap.

The specific surface areas of prepared samples and TiO_2 were determined using the BET method respectively from krypton and nitrogen adsorption isotherms measured at 77 K (BEL JAPAN, Inc., BELSORP 18PLUS-SP, BELSORP-mini).

2.3. Photocatalytic Activity Measurement. The photocatalytic activity of the catalyst was examined using a gas-closed circulation system equipped with a GC-TCD (Shimadzu, GC-8A). Powdered 1 wt % RuO_2/SAN (0.5 g), SAN (0.5 g), or TiO_2 (0.5 g) was dispersed into a 10 vol % methanol aqueous solution (500 mL) in an inner-irradiation-type reaction cell made of Pyrex glass. The reaction cell was connected to the gas-closed circulation system. After deaeration of the dispersion with stirring using a magnetic stirrer, Ar gas was introduced into the reactor (1.3×10^4 Pa). Then, the dispersion was irradiated with a 100 W high-pressure mercury lamp, and the amount of H_2 evolved was measured by the GC-TCD. According to the same procedure, the amount of O_2 evolved from a 0.01 M AgF aqueous solution (500 mL) was measured using the powdered catalysts (0.3 g) in a He atmosphere (1.3×10^4 Pa).

3. Results and Discussion

3.1. Cation Arrangement at the B Site in Sr−Al−Nb−O Double Perovskite. Figure 2 shows PXRD patterns of SAN perovskites prepared using the solid-state reaction with various calcination temperatures for 10 h. After calcination at 1200 and 1300 °C, $Sr_5Nb_4O_{15}$ was clearly observed as an impurity phase in addition to the perovskite phase, and the intensity of the diffraction lines from $Sr_5Nb_4O_{15}$ decreased with increasing calcination temperature. Considering the stoichiometry, impurity phases other than $Sr_5Nb_4O_{15}$ might be present below 1300 °C, though they were not detected by PXRD. At 1400 °C, diffraction lines from any impurity phases eventually disappeared, and the PXRD pattern was ascribable to the cubic perovskite-type structure. At a calcination temperature of 1500 °C, additional diffraction lines from impurities, such as $SrAl_2O_4$, were observed, and the amount of impurity phases depended on the calcination procedure. When the single-phase SAN, which was obtained at 1400 °C, was additionally calcined at 1500 °C (Figure 2e), weak but clear diffraction lines of impurity phases were observed. This indicates that the decomposition of SAN perovskite proceeds at a temperature of 1500 °C. When the solid-state mixture was directly calcined at 1500 °C (Figure 2d), the amounts of impurity phases were larger than those of the product after two-step calcination (Figure 2e). According to the phase diagrams of $SrO-Nb_2O_5$, $SrO-Al_2O_3$, and $Al_2O_3-Nb_2O_5$ systems,[34,35] the liquid phase appears over 1410 ± 10 °C for the $Al_2O_3-Nb_2O_5$ system around the stoichiometry. When the solid-state mixture of the starting materials is directly heated to 1500 °C, as in the case shown in Figure 2d, impurity phases of mixed oxides and unreacted single oxides will be formed or present at lower temperatures. If they survive above *ca.* 1400 °C, the Al−Nb−O liquid phase will be formed. The appearance of the liquid phase may cause volatilization of the components and lead to the formation of a large amount of impurities. It is noted that the calcination temperatures used in this study were lower than the melting temperature of SAN, 1790 °C.[36] The results mentioned above clearly indicate that a calcination temperature of 1400 °C is suitable for the formation of single-phase SAN perovskite because a temperature of 1300 °C is too low to form the single phase under the present synthesis conditions, and the decomposition of SAN proceeds at 1500 °C.

It has been reported that a cubic ordered double perovskite with rock-salt ordering of B cations has a superlattice structure with unit cell dimensions of $2a_p \times 2a_p \times 2a_p$: a_p is the lattice constant of cubic perovskite of a primitive ABO_3 type.[12] According to indexing based on the superlattice structure, the appearance of 111, 311, 331, and 511 diffraction lines, namely, superlattice diffraction lines, is evidence of the rock-salt ordering of B cations.[12] As shown in Figure 2c, all of the diffraction lines were indexed on the basis of the superlattice structure, indicating that SAN prepared at 1400 °C for 10 h contained the ordered phase with an alternate arrangement of Al^{3+} and Nb^{5+}.

The effect of the calcination time was investigated for the synthesis of SAN at 1400 °C (Figure 3). Although all of the samples calcined for 10 to 50 h were single-phase cubic perovskites, relative intensities (I/I_0) of the superlattice diffraction lines tended to increase with increasing calcination time. The superlattice diffraction lines arise from the ordered arrangement of B cations as stated above, and the strongest line with an intensity of I_0 is contributed by both the 220 and 110 diffractions of the ordered and disordered phases, respectively. This means that the value of I/I_0 of the superlattice diffraction lines includes information about the degree of cation-ordering at the B site. Therefore, the results in Figure 3 showed that

(34) Levin, M. E.; McMurdie, F. H. *Phase Diagrams for Ceramists Vol. 3*; The American Ceramic Society: Westerville, OH, 1975.
(35) Roth, S. R.; Dennis, R. J.; McMurdie, F. H. *Phase Diagrams for Ceramists Vol. 5*; The American Ceramic Society: Westerville, OH, 1987.
(36) Brandle, D. C.; Fratello, J. V. *J. Mater. Res.* **1990**, *5*, 2160.

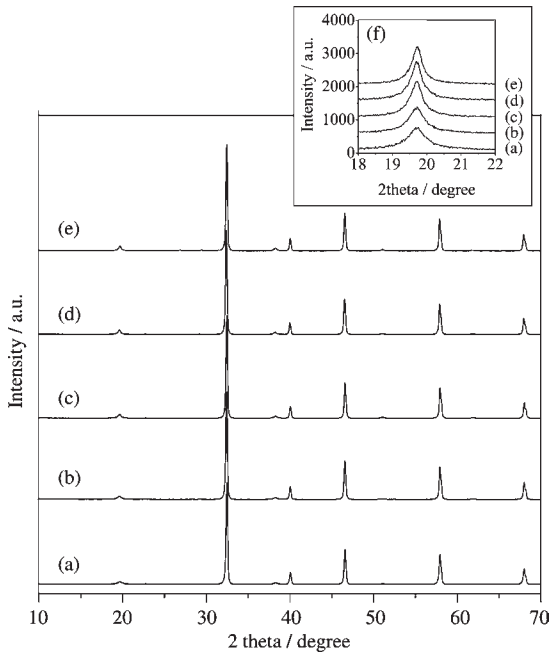

Figure 3. PXRD patterns of Sr−Al−Nb−O double perovskites calcined at various calcination times at 1400 °C. (a) 10 h, (b) 20 h, (c) 30 h, (d) 40 h, (e) 50 h, (f) the enlarged 111 superlattice diffraction lines of a−e.

the degree of cation-ordering at the B site increased with increasing calcination time.

TEM observations were performed to investigate the structure of SAN in detail. Figure 4 shows the TEM images of SAN calcined at 1400 °C for 30 h. The selected area of the particle in Figure 4a gave electron diffraction (ED) spots (Figure 4b), and therefore the single crystal was formed in the observed area. The distances of the crystal plane ($d_{\{hkl\}}$) calculated from the ED pattern ($d_{\{111\}}$ = 0.46 nm, $d_{\{200\}}$ = 0.40 nm, $d_{\{113\}}$ = 0.25 nm, $d_{\{220\}}$ = 0.29 nm) agreed with those of the crystal plane calculated from the PXRD pattern ($d_{\{111\}}$ = 0.450 nm, $d_{\{200\}}$ = 0.389 nm, $d_{\{113\}}$ = 0.234 nm, $d_{\{220\}}$ = 0.275 nm), indicating that the particle was made of a single-phase perovskite-type oxide. The appearance of 111 and 113 superlattice ED spots proved the existence of the ordered phase in the particle, as in the PXRD results. Dark field observation is a useful method for determining the domain which gives an ED spot. For the B-site ordered double perovskite, dark field observations using the 111 superlattice diffraction spot were performed to distinguish the domain of the completely B-site ordered structure.[37] The dark field image of the particle is shown in Figure 4c, and the observation clarified that the completely B-site ordered domain existed in the near-surface region of the particle (bright area in Figure 4c). On the basis of PXRD measurements and TEM observations, it has been confirmed that the SAN crystallite consisted of two domains of completely B-site ordered Sr_2AlNbO_6 and disordered $SrAl_{0.5}Nb_{0.5}O_3$, and the Sr_2AlNbO_6 domain in a crystallite expands with increasing calcination time. Randall et al. have reported a similar trend of expansion of the ordered-phase domain for the Pb_2ScTaO_6 single crystal.[37]

(37) Randall, A. C.; Barber, J. D.; Whatmore, W. R.; Groves, P. *J. Mater. Sci.* **1986**, *21*, 4456–4462.

Rietveld analysis was performed to determine the degree of cation-ordering in SAN. So far, the degree of cation-ordering in $A_2BB'O_6$ has been determined by Rietveld analysis using the structural model $A_2(B_xB'_{1-x})(B'_xB_{1-x})O_6$ ($0.5 \leq x \leq 1.0$), where x means the occupancy of B and B′ cations at their original sites. The degree of cation-ordering has been defined by eq 1 using a refined x value;[13−17] x = 1.0 and 0.5 correspond respectively to completely ordered and disordered phases.

$$\text{The degree of cation- ordering at the B site} = 2 \times |100x - 50|/\% \quad (1)$$

The calculation model was based on the single-phase $A_2(B_xB'_{1-x})(B'_xB_{1-x})O_6$ and set one value of full width at half-maximum (fwhm) for all of the diffraction lines. TEM observation clearly indicated that the SAN prepared in this study was a mixture of Sr_2AlNbO_6 (space group: $Fm\bar{3}m$) and $SrAl_{0.5}Nb_{0.5}O_3$ (space group: $Pm\bar{3}m$). In addition, fwhm values of superlattice lines were different from those of the other lines, as shown in Figure 5 for the 111 and 220 diffraction lines of SAN prepared at 1400 °C for 30 h. The larger fwhm values of the superlattice 111 diffraction mean that the crystallite (domain) size of the Sr_2AlNbO_6 ordered phase is smaller than that of $SrAl_{0.5}Nb_{0.5}O_3$, and this is consistent with the TEM observation. The above discussion clearly suggests that not the conventional single-phase model but the new mixed-phase model should be applied for Rietveld analysis in the present case. The refinement with the mixed-phase model is done for the mixture of $y(Sr_2AlNbO_6)$ and $(1-y)(SrAl_{0.5}Nb_{0.5}O_3)$, where y is a mass fraction of the ordered phase and therefore corresponds to the degree of ordering in SAN. In the mixed-phase model, different fwhm values can be set for different phases, and cell parameters for each phase can be refined.

The representative results of Rietveld analysis by the mixed-phase model are shown in Figure 6 and Table 1 for SAN calcined for 30 h at 1400 °C. The results showed that Sr_2AlNbO_6 and $SrAl_{0.5}Nb_{0.5}O_3$ phases both had a cubic unit cell, and the lattice constant of the ordered phase was nearly double that of the disordered phase, as expected. In order to confirm the validity of the mixed-phase model, the Rietveld refinement using the conventional single-phase model was performed, and the result was compared with that using the mixed-phase model. The refinement using the conventional model was possible with a goodness-of-fit indicator (S) of 2.2. The S value in the mixed-phase model refinement was 1.9 (Table 1), and therefore the new model was more valid than the conventional model. In the present study, the new model was used to refine the crystal structure of SAN.

Figure 7 shows the dependence of the fraction of Sr_2AlNbO_6 on calcination time at 1400 °C. With increasing the calcination time, the fraction increased linearly to 44% up to 30 h and then leveled off to reach 48% after 50 h, indicating that the growth of the ordered phase is almost completed after calcination for 30 h under the present synthesis conditions. Woodward et al. reported that the degree of cation ordering depended on the calcination temperature, and it was 94% for SAN synthesized by a flux method with calcination at 1400 °C.[17] The difference in the fraction of the ordered phase might arise

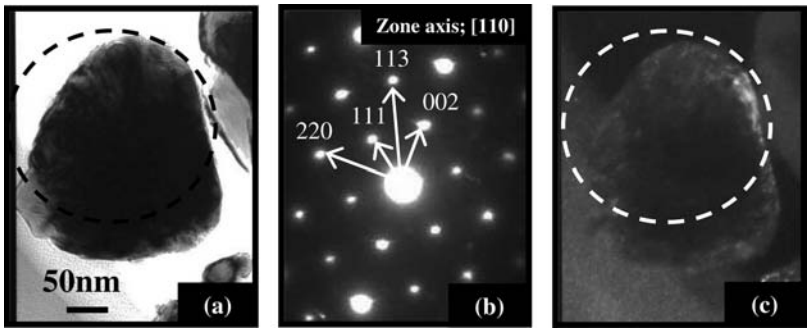

Figure 4. TEM images of Sr−Al−Nb−O double perovskite calcined for 30 h at 1400 °C. (a) Bright field image, (b) electron diffraction pattern, (c) dark field image using 111 diffraction.

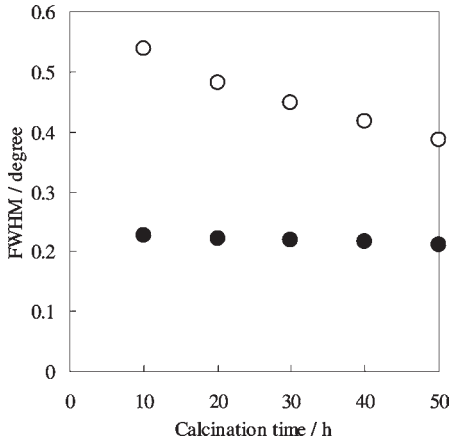

Figure 5. Dependence on calcination time at 1400 °C of fwhm of (111) and (220) diffraction lines from Sr−Al−Nb−O double perovskites. Open circle, 111 diffraction line; filled circle, 220 diffraction line.

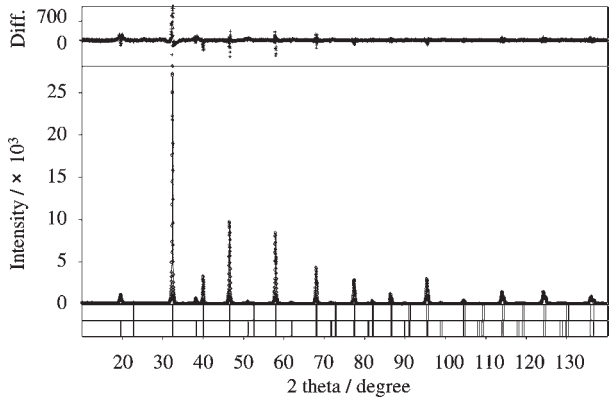

Figure 6. Result of Rietveld analysis for Sr−Al−Nb−O double perovskite calcined for 30 h at 1400 °C.

from the different preparation methods used. Two B-site cations of Al^{3+} and Nb^{5+} ions in the ordered SAN phase are arranged alternately, and therefore it is reasonably accepted that a preparation method with more homogeneous mixing of Al and Nb precursors gives the ordered phase more easily. The flux method is well-known to facilitate the formation of mixed metal oxides. In the present solid state reaction method, Al_2O_3, Nb_2O_5, and $SrCO_3$ were used as starting materials. The diffusion of cations in the solid is required to form the mixed metal oxide phase, and the presence of Al and Nb in the 1:1 ration is indispensable in forming the ordered phase. The

Table 1. Result of Rietveld Analysis for Sr−Al−Nb−O Double Perovskite Calcined for 30 h at 1400 °C[a]

$SrAl_{0.5}Nb_{0.5}O_3$ (SG: $Pm\bar{3}m$)						
a = 0.389575(5) nm						
	site	g	x	y	z	B (Å^2)[b]
O	3d	1	1/2	0	0	0.83(7)
Sr	1b	1	1/2	1/2	1/2	0.73(2)
Al	1a	1	0	0	0	0.40(2)
Nb	1a	1	0	0	0	0.40(2)
R_F = 1.24%, R_I = 1.78%, mass fraction = 0.5553						
Sr_2AlNbO_6 (SG: $Fm\bar{3}m$)						
a = 0.77955(17) nm						
	site	g	x	y	z	B (Å^2)[b]
O	24e	1	0.2489(5)	0	0	0.83
Sr	8c	1	1/4	1/4	1/4	0.73
Al	4b	1	1/2	1/2	1/2	0.40
Nb	4a	1	0	0	0	0.40
R_F = 3.34%, R_I = 5.14%, mass fraction = 0.4447						

[a] R_{wp} = 12.10%, R_p = 7.75%, R_R = 10.29%, R_e = 6.34%, S = 1.9. [b] B values were refined using Rietveld analysis for $SrAl_{0.5}Nb_{0.5}O_3$, and the obtained values were used for Sr_2AlNbO_6.

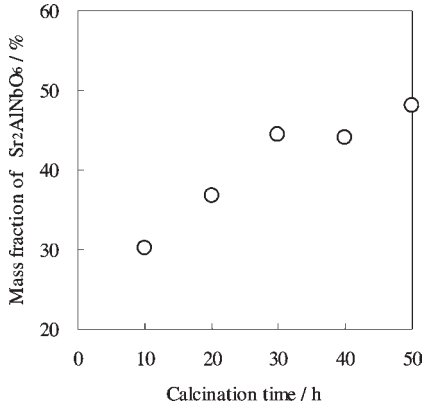

Figure 7. Relationship between the calcination time and the mass fraction of the ordered Sr_2AlNbO_6 in Sr−Al−Nb−O double perovskites refined by Rietveld analysis. Sr−Al−Nb−O perovskites were calcined at 1400 °C.

calcination time dependence of the fraction (Figure 7) implies that the disordered phase is first formed (kinetically favored) and that it is gradually transformed

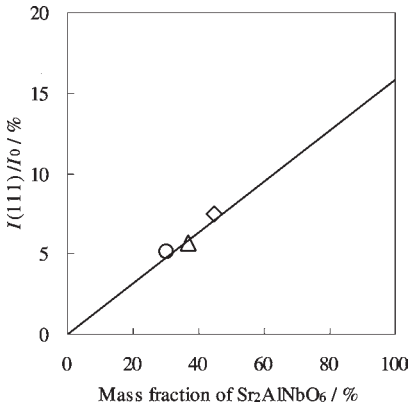

Figure 8. Relationship between the mass fraction of the ordered Sr_2AlNbO_6 phase and the relative intensity of the 111 diffraction line for Sr−Al−Nb−O double perovskites prepared at 1400 °C for 10 h (open circle), 20 h (open triangle), and 30 h (open square). Solid line, theoretical line based on the mixed-phase model (see text for detail).

to the thermodynamically favored ordered phase until reaching the equilibrium value under the conditions given.

As stated above, the I/I_0 value of the superlattice diffraction lines can be used to determine the fraction of the ordered phase. The mass fraction of Sr_2AlNbO_6 in the mixed-phase model principally has a proportional relation to a value of I/I_0. This relation is show in Figure 8 for the 111 diffraction line: the $I(111)/I_0$ value at the 100% ordering (15.8%) was calculated on the basis of the crystal data of Sr_2AlNbO_6 and drew a straight line passing through the origin and the calculated value of the 100% ordering. The experimental results of SAN perovskites calcined at 1400 °C are also plotted in Figure 8, and they were practically on the theoretical line, indicating that the observed $I(111)/I_0$ value can be directly transformed to the fraction of Sr_2AlNbO_6 by using the relation. SAN perovskites were synthesized at 1400 °C several times with the same method and under the same conditions. As shown in Table 2, the fractions of the ordered phase in prepared SAN perovskites were 30% according to the Rietveld refinement and 31 and 30% according to the estimation from Figure 8 after a calcination time of 10 h, 37% (refinement) and 36% (estimation) after 20 h of calcination, and 44% (refinement) and 42 and 47% (estimation) after 30 h of calcination. These reasonably close values for each case clearly indicate the good reproducibility of the preparation as well as the validity of the estimation from the linear relationship between the relative intensity of the superlattice diffraction and the fraction of the ordered phase.

3.2. Optical Absorption Property. Figure 9 shows the UV−vis DRS of SAN perovskites with various fractions of Sr_2AlNbO_6. The observed photon energy at the absorption edges, namely optical band gap, for SAN perovskites was 4.1 eV for all of the samples. The identical optical band gap of SAN perovskites with different ordered phase fractions does not necessarily mean that ordered Sr_2AlNbO_6 and disordered $SrAl_{0.5}Nb_{0.5}O_3$ have the same optical band gap. Since SAN perovskites prepared in this study are a mixture of ordered and disordered phases, the absorption spectrum at longer wavelengths and the estimated band gap from the portion are governed by the phase with smaller band gap. It has been reported that the optical band gap of perovskite-type oxide is mainly determined by the kind of B cation and the −B−O−B− bond angle.[9,38] The effects of these factors, however, are not so important for the optical band gap of SAN because Sr_2AlNbO_6 and $SrAl_{0.5}Nb_{0.5}O_3$ include Al^{3+} and Nb^{5+} cations at the same molar ratio, and the −B−O−B− angles in the both structures are 180°. Regarding the relationship between cation arrangement and band structure of the perovskite-type oxide, Eng et al. have investigated the effect of the isolation of the TaO_6 octahedron on the optical band gap by comparing $KTaO_3$ and Sr_2AlTaO_6. The band gap of Sr_2AlTaO_6 was larger than that of $KTaO_3$, and they suggested that the isolation of the TaO_6 octahedron by the AlO_6 octahedron is the origin of the increase of the optical band gap.[38] To the best of our knowledge, however, the relationship between the arrangement of two B cations (Al and Nb in the present SAN) and the optical band gap has not been investigated. Considering the cation isolation discussion, ordered Sr_2AlNbO_6 with a complete isolation of the NbO_6 octahedron by the AlO_6 octahedron might have a larger band gap than disordered $SrAl_{0.5}Nb_{0.5}O_3$, in which the linkage of the NbO_6 octahedra is present. This inferred difference of optical band gap might be true if one considers that disordered $SrAl_{0.5}Nb_{0.5}O_3$, which is the major phase in SAN perovskites, dominates the absorption spectrum at longer wavelengths. The relationship between the cation arrangement and the band gap should be determined experimentally by using, for example, a completely ordered material or theoretically by the calculation of the band structure.

3.3. Photocatalytic Property. The results of the photocatalytic reactions performed in this study are summarized in Table 2. The photocatalytic H_2 and O_2 evolutions from an aqueous methanol solution and an aqueous AgF solution, respectively, were observed with SAN perovskites with and without a RuO_2 cocatalyst, and no change of the crystal structure of SAN perovskites was noticed from PXRD measurements of fresh and used catalysts. These results indicate that SAN works as a photocatalyst, and this is the first report to reveal the photocatalytic activity of the SAN perovskite.

Time courses of photocatalytic H_2 evolution from a 10 vol % methanol aqueous solution over SAN and 1 wt % RuO_2/SAN are shown in Figure 10. The amount of H_2 evolution increased with increasing reaction time over SAN perovskites both with and without the cocatalyst. The amount of H_2 evolved up to 8 h decreased with an increase in the calcination time, and this trend was held after normalization via specific surface area (S_a; Table 2a). In most of the powdered photocatalysts, a cocatalyst has been used to improve the photocatalytic activity.[2] In this study, RuO_2, which has been reported to show the functionality of a cocatalyst,[39,40] was supported on SAN. As shown in Figure 10, the amount of photocatalytic H_2 evolution was greatly increased over 1 wt % RuO_2/SAN as compared with the bare SAN, confirming

(38) Eng, W. H.; Barnes, W. P.; Auer, M. B.; Woodward, M. P. *J. Solid State Chem.* **2003**, *175*, 94–109.
(39) Sakata, T.; Hashimoto, K.; Kawai, T. *J. Phys. Chem.* **1984**, *88*, 5214–5221.
(40) Inoue, Y.; Kubokawa, T.; Sato, K. *J. Phys. Chem.* **1991**, *95*, 4059–4063.

Table 2. Results of the Photocatalytic Reactions over Sr−Al−Nb−O Double Perovskite

(A) H_2 evolution from an aqueous methanol solution over catalysts (0.5 g)

catalyst	calcination time/h	$I(111)/I_0$[b]/%	F_{op}[c]/%	S_a/m^2 g^{-1}	H_2 evolution[a]	
					μmol	μmol (m^2 cat)$^{-1}$
Sr−Al−Nb−O	10	5.1	30[d]	3.1	6.0	3.9
	20	5.7	37[d]	3.0	2.5	1.7
	30	7.5	44[d]	2.9	1.6	1.1
1 wt % RuO_2/ Sr−Al−Nb−O	10	5.1	31[e]	3.2	26.7	16.8
	20	5.9	36[e]	2.9	19.3	13.4
	30	7.0	42[e]	2.7	16.6	12.4
TiO_2				55.3	24.9	0.9

(B) O_2 evolution from an aqueous AgF solution over catalysts (0.3 g)

catalyst	calcination time/h	$I(111)/I_0$[b]/%	F_{op}[c]/%	S_a/m^2 g^{-1}	O_2 evolution[a]	
					μmol	μmol (m^2 cat)$^{-1}$
Sr−Al−Nb−O	10	4.9	30[e]	3.4	20.5	20.2
	20	5.7	37[d]	2.9	12.0	13.8
	30	7.8	47[e]	3.6	9.1	8.5
1 wt % RuO_2/ Sr−Al−Nb-O	10	5.1	31[e]	3.2	21.6	22.7
	20	5.9	36[e]	2.9	12.0	13.9
	30	7.0	42[e]	2.7	9.0	11.1
TiO_2				55.3	1153.8	69.5

[a] Gross and surface-area normalized amount of gas evolved after 8 h of photoirradiation. [b] Relative intensity of the 111 diffraction line. [c] Mass fraction of the ordered Sr_2AlNbO_6 phase. [d] Refined by Rietveld analysis. [e] Estimated from the $I(111)/I_0 - F_{op}$ relation (Figure 8).

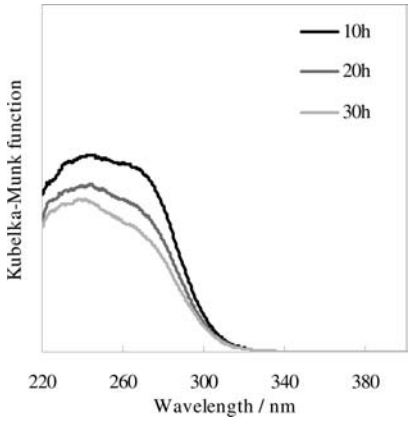

Figure 9. Absorption spectra of Sr−Al−Nb−O double perovskites calcined for 10, 20, and 30 h at 1400 °C.

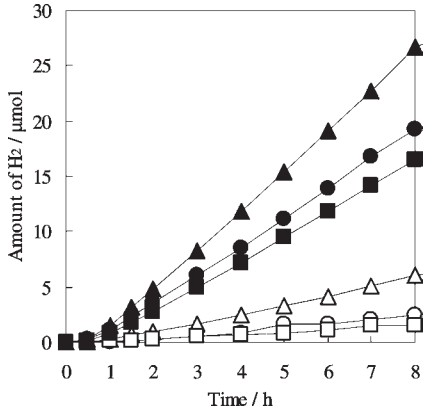

Figure 10. Time course of the H_2 evolution from a 10 vol % methanol aqueous solution over Sr−Al−Nb−O double perovskites calcined at 1400 °C. Calcination time: 10 h (triangle), 20 h (circle), 30 h (square). Open symbols, bare SAN; filled symbols, 1 wt % RuO_2/SAN.

the cocatalytic function of RuO_2 on the SAN photocatalyst. As in the case of bare SAN perovskites, the amount of H_2 evolved over 1 wt % RuO_2/SAN also decreased when the calcination time of SAN was prolonged. The agreement of the activity order over the catalysts with and without RuO_2 implies that the dependence of the activity on the calcination time is governed mostly by the bulk property.

A photocatalytic reaction with an aqueous AgF solution was also performed. The evolution of O_2 was observed (Table 2b), and the formation of Ag metal was confirmed by PXRD after the reaction. The amount of O_2 evolved increased in proportion to the photoirradiation time, up to 8 h over SAN and 1 wt % RuO_2/SAN. However, the cocatalytic function of RuO_2 was negligible for the reaction. The amounts of O_2 evolved on both gross and S_a-normalized bases decreased with increasing calcination time. Since the same dependence was observed in both H_2 and O_2 evolution reactions, the dependence of the activity on the calcination time originates from the bulk property of SAN irrespective of the kind of reactions.

As described in section 3.1, the mass fraction of ordered Sr_2AlNbO_6 in SAN increased with increasing calcination time. The amounts of gases evolved up to 8 h of photoirradiation are plotted as a function of the mass fraction of ordered Sr_2AlNbO_6 in Figure 11. The photocatalytic activity of SAN decreased with an increase in the fraction of Sr_2AlNbO_6, indicating that the photocatalytic activity of disordered $SrAl_{0.5}Nb_{0.5}O_3$ should be higher than that of ordered Sr_2AlNbO_6. The relation was not straight, and the decrease in the lower fraction range seemed to be larger than that at the higher fraction range. This might be reasonable from the TEM observation that the less active ordered phase is formed from the near-surface region of particles of the active disordered phase.

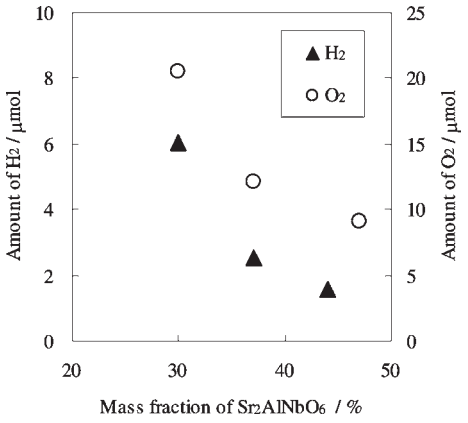

Figure 11. The relationship between the mass fraction of Sr_2AlNbO_6 in Sr−Al−Nb−O double perovskite and the amounts of the gas evolved after photoirradiation for 8 h. A total of 0.5 g of SAN was used for the photocatalytic H_2 evolution from an aqueous methanol solution, and 0.3 g of SAN was used for the photocatalytic O_2 evolution from an aqueous AgF solution.

In order to evaluate the activity level of the newly developed catalyst, the photocatalytic activity of bare SAN was compared with that of TiO_2. If the surface area−normalized activity of the most active SAN after calcination for 10 h was used, the activity of SAN was 4.3 times higher and 3.4 times lower than TiO_2 for H_2 and O_2 evolution, respectively. Roughly speaking, it can be said that the activity of the newly developed SAN is on the same level as TiO_2.

The present study revealed, for the first time, the effect of the cation ordering on the catalytic activity with the catalysts of the same constituent metal cations. The disordered phase was inferred to be more active than the ordered phase, although the reason for that will be clarified in future studies.

4. Conclusion

In this study, Sr−Al−Nb−O double perovskite (SAN) was synthesized using the conventional solid-state reaction method, and its structure and photocatalytic properties were investigated from a viewpoint of cation-ordering at the octahedral B site. TEM observations confirmed that SAN particles have a domain structure with disordered $SrAl_{0.5}Nb_{0.5}O_3$ and ordered Sr_2AlNbO_6 phases and that the latter domain was preferentially present at the surface region of the particles of the former phase. The fraction of the ordered phase was estimated from the newly proposed mixed-phase model for Rietveld analysis and the relative intensity of the superlattice PXRD line. The photocatalytic activity of SAN for both H_2 evolution from an aqueous methanol solution and O_2 evolution from an aqueous AgF solution were found to increase with the decreasing fraction of the ordered phase. The present study revealed the effect of the cation ordering on the photocatalytic activity of mixed metal oxides, and the origin of the relation between the cation arrangement and catalytic activity will be made clear in future works.

Acknowledgment. This work was supported by a Grant-in-Aid for Scientific Research on Priority Areas (Nos. 19028050 and 20037053, "Chemistry of Concerto Catalysis") from the Ministry of Education, Culture, Sports, Science and Technology, Japan and a grant from the Global-Centre of Excellence in Novel Carbon Resource Sciences, Kyushu University. The authors thank Dr. K. Yoshida for valuable discussions.